ELSEVIER

Chemical Engineering Journal 72 (1999) 139–151

Chemical Engineering Journal

Flowrate quantification of the pumped-air stream from a 63 mm diameter centrifugal wheel atomiser

R.A. Stafford[a], D.H. Glass[a,*], R.T. Leah[b]

[a]*Department Of Chemical Engineering, The University of Edinburgh, King's Buildings, Mayfield Rd, Edinburgh, EH9 3JL, UK*
[b]*Department of Chemical Engineering, The University Of Birmingham, Birmingham, UK*

Received 2 February 1996; received in revised form 30 October 1998; accepted 4 November 1998

Abstract

The air-pumping characteristic of a 63 mm diam centrifugal atomiser running dry within a cocurrent spray dryer was studied extensively using a novel experimental technique which involved the direct measurement of the wheel vacuum pressure together with the power required to pump the air. Approximately 10% of the power consumed by the atomiser was utilised in pumping the airstream. A further 25% was consumed in shearing the air around the wheel and the remaining 65% was consumed by friction and motor losses within the drive train. Typically, the wheels considered pumped between 2 l s^{-1} and 6.5 l s^{-1} of air at a maximum rotational speed of 50 000 rpm which corresponded to between 5% and 16% of the primary air supply to the dryer. A dynamic closure of the wheel/atomiser body gap was observed occurring at 30 000 rpm to 40 000 rpm which was thought to be due to an upward acting force generated by the pressure differential either side of the wheel. This significantly affected the air-pumping behaviour of the wheel.

Keywords: Air-pumping; Centrifugal atomisers; Fluid flow; Spray drying

1. Introduction

Centrifugal wheel atomisers are used throughout the process and allied industries to produce a spray of relatively small mean droplet diam. A typical application of such an atomiser is the atomisation of feedstock during the spray drying process. The principle of operation of centrifugal atomisers involves the addition of energy in the form of centrifugal energy to the liquid feed in order to produce an increase in surface area. The liquid is fed onto a rapidly rotating surface and the action of the rotation is to throw the liquid radially outwards from the axis of rotation, thereby imparting energy into the liquid. Disintegration of the liquid film results in the formation of a stream of droplets. In the case of a wheel atomiser the rotating surface is a thick disc which has radial ports machined around its circumference which are fed from a central cavity.

A detrimental effect of wheel rotation is the generation of a region of low air pressure at the wheel centre as illustrated in Fig. 1 [1]. This region establishes an air flow which flows radially inward through the clearance gap between the wheel and the atomiser body and upon reaching the cavity in the wheel centre, the flow then changes direction and flows radially outwards through the ports. This air stream typically draws air from the hot air inlet in the roof of the dryer and this can simultaneously aerate and partially dry the feedstock within the atomiser wheel. These effects are detrimental to the operation of the spray dryer as feedstock aeration can lead to an increase in product porosity and a decrease in bulk density. Dried particles deposited on or within the wheel will overdry and can constitute a source of product contamination and a potential ignition source for fire and explosions [2]. Lastly, the pumped airstream, which possesses a large amount of radial momentum, can significantly affect the dryer flow pattern in pilot plants of up to 2 m in diam [3].

In order to numerically simulate the dryer flow field using for example a computational fluid dynamics code, it is essential to include the pumped airstream as a mass flow inlet boundary condition [4]. To do this a means of estimating the mass flowrate for a wheel operating under a given set of conditions is required. Little data relating to this is available in the open literature. During the course of conducting such modelling [4], an estimate of the pumped air stream flowrate was made from data described by Keey et al.

*Corresponding author. Fax: +44-0131-650-6551; e-mail: don.glass@ed.ac.uk

1385-8947/99/$ – see front matter
PII: S1385-8947(98)00144-2

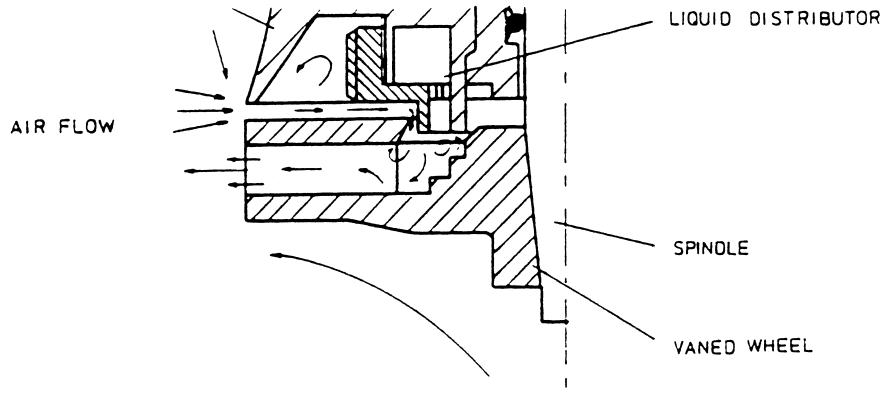

Fig. 1. Air-pumping circuit within a centrifugal wheel atomiser [1].

[5]. In this study the authors considered a 120 mm diam wheel by estimating the power required to pump the air and using this value within a numerical model of the atomiser to estimate the pumped-air flowrate. Their conclusions were that at speeds of 21 800 rpm and 24 000 rpm in air at room temperature and at 200°C, the air flowrates corresponded to 7% (28 l s^{-1}) and 17% (58 l s^{-1}) of the primary air flow through the dryer. The measurement of pumping power was made by taking the difference in the power consumption, with and without the wheel fitted. This ignores the power consumed in shearing the fluid on the upper and lower surfaces of the wheel which does not contribute to the centrifugal pumping action.

The present work was aimed at a more explicit measurement of the flowrate of the pumped airstream in the absence of a liquid spray, by measuring the power required to pump the airstream, taking account of the shearing power described above, together with the measurement of the vacuum pressure at the wheel centre. In this way a direct estimate of the flowrate was made and by using wheels with a differing number and size of radial ports together with a range of air gaps, the influence of these parameters on air pumping was quantified.

2. Equipment

A CE-63 wheel atomiser (APV Anhydro A/S, Copenhagen, Denmark) was investigated which consisted of a 63 mm diam wheel driven by a 500 W electric motor via a pair of parallel spur gears at speeds up to 50 000 rpm. Four different wheels were considered which had differing numbers of ports and port diam, namely, 2 × Ø2 mm; 4 × Ø2 mm; 8 × Ø2 mm; and 4 × Ø4 mm. Fig. 2 shows the schematic diagram of the wheel with 4 mm diam ports. The other wheels differed from this only in the number and diam of the ports. The atomiser was located within the roof air disperser unit of an APV Anhydro Laboratory No. 1 pilot plant spray dryer which was supplied with unheated air nominally at 40°C and 0.04 m^3 s^{-1}.

The wheel vacuum pressure was measured with a digital micromanometer fitted to the pipe within the atomiser which would normally be used to pass feedstock to the central cavity of the wheel as shown in Fig. 3. The atomiser speed was controlled by an auto transformer fitted to the motor electrical supply and the wheel speed was measured using an inductive transducer fitted to the wheel drive train. This allowed the wheel speed to be measured to within 10 rpm. The electrical power consumption to the atomiser was measured using a clamp wattmeter fitted to the motor supply lead together with a supply voltage connection from the autotransformer. This configuration took a direct account of the electrical supply power factor.

3. Method

The power drawn by the atomiser motor was consumed in three principal ways:

1. Frictional losses in the motor and drive train gears and bearings, W_f
2. Power required to shear the air along the circumference and upper and lower surfaces of the wheel, W_s
3. Power required to pump the air through the radial ports, W_p.

W_f was measured by running the atomiser without the wheel and measuring the power consumed. W_s was calculated by running the atomiser with the wheel fitted but with the ports sealed. By deducting W_f from the measured power, W_s was calculated. W_p was calculated by running the atomiser with the wheel fitted and the holes unblocked. By deducting ($W_f + W_s$) from the measured power, W_p was calculated. Fig. 4 shows the variation of measured friction, shear and pumping power with speed for the 4 × Ø4 mm wheel. It should be noted that at 50 000 rpm, the three power values are typically $W_f \approx 130$ W, $W_s \approx 50$ W and $W_p \approx 20$ W, respectively. Hence the assumption made by Keey et al. [5] in not separating the shear power (W_s) from the pumping power (W_p) would result, in this case, in an overestimation of pumping power by 350% which would introduce a substantial error.

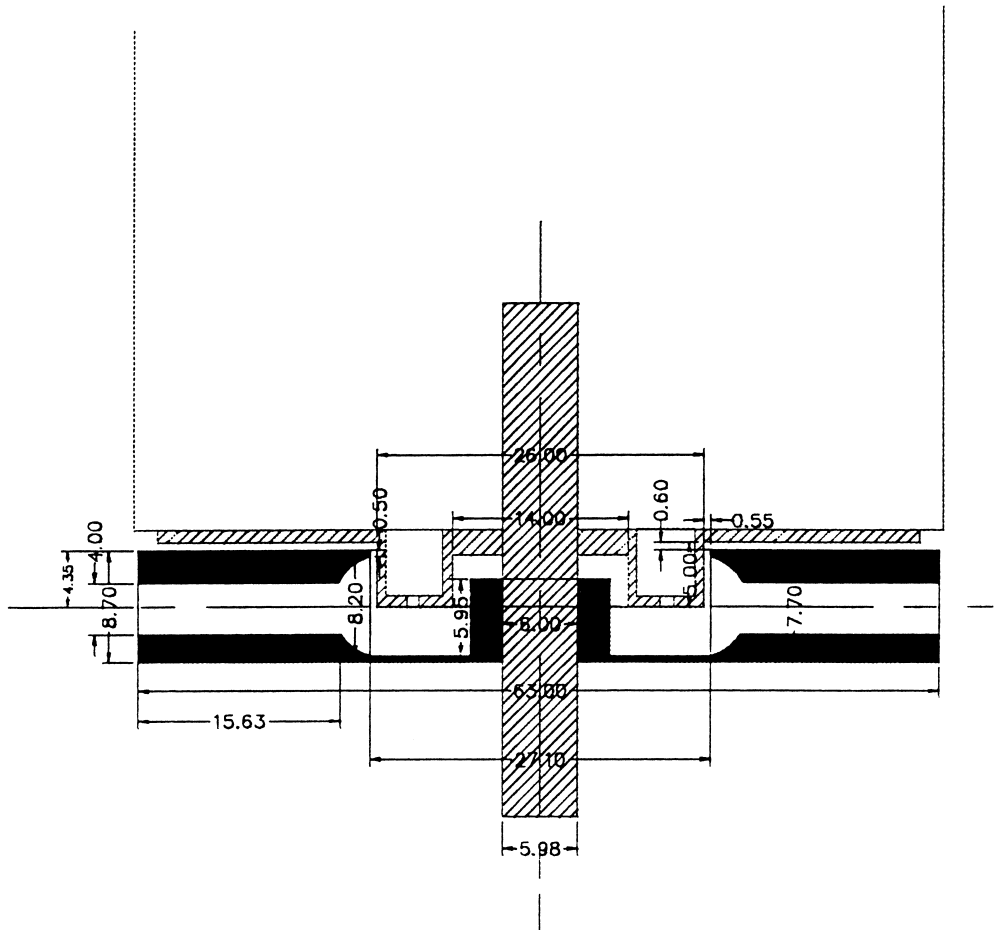

Fig. 2. Cross-section of an APV Anhydro A/S CE63 atomiser wheel showing detail of the port and gap geometry.

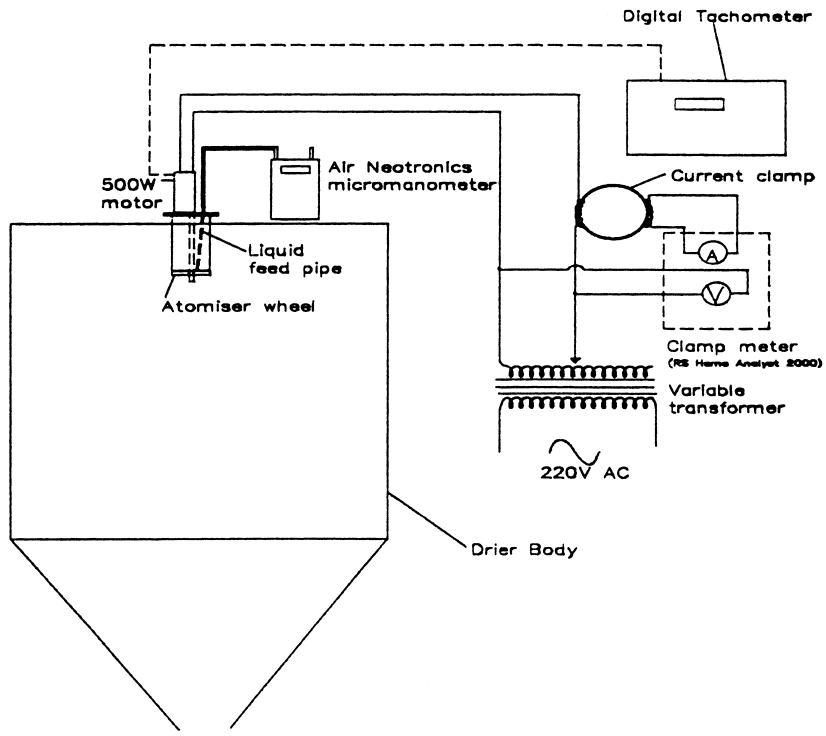

Fig. 3. Schematic of equipment used showing atomiser location and connection of instrumentation.

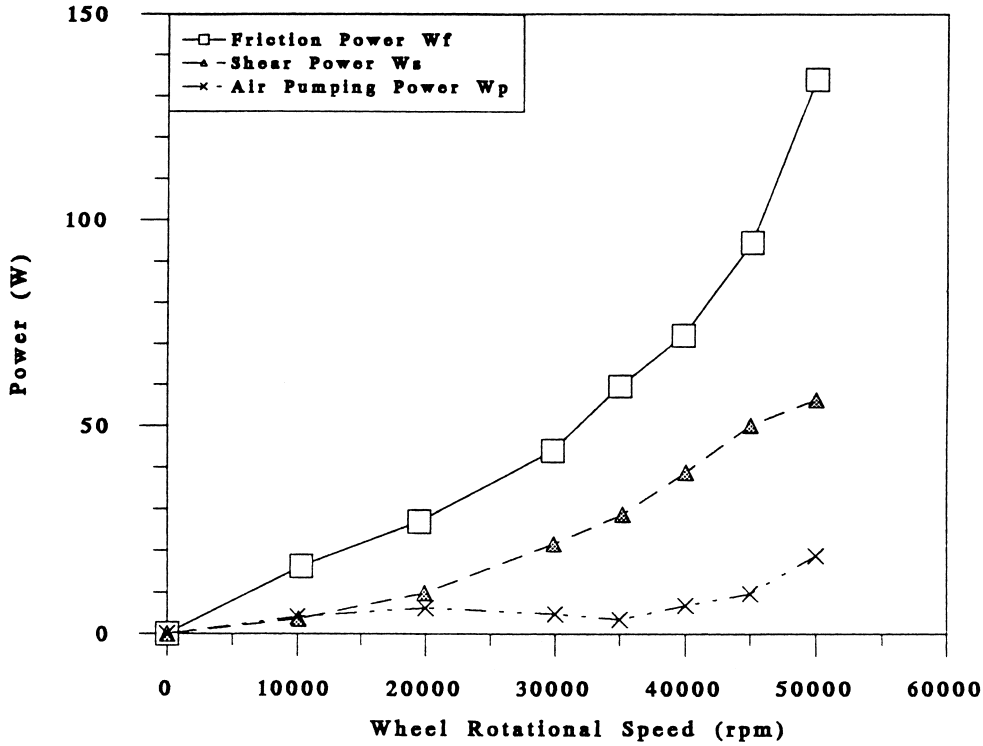

Fig. 4. Friction power W_f, shear power W_s and air pumping power W_p for the atomiser wheel with 4 × Ø4 mm ports. Air gap, $x = 0.6$ mm.

The pressure difference across the wheel Δp_1 which caused air to be drawn in to the wheel centre through the air gap was calculated from the measured chamber pressure p_{ch} and the measured pressure at the wheel centre, p_w,

$$\Delta p_1 = p_{ch} - p_w \tag{1}$$

p_{ch} was measured with the wheel stationary and p_w with the wheel rotating at the appropriate speed.

As the flow velocities within the wheel ports were high it was considered that compressibility effects were liable to be significant. To this end, the air pumping process was considered as an adiabatic compression process, hence the pumped air flowrate Q was estimated using W_p, p_{ch} and p_w [6],

$$W_p = Qp_1 \frac{\gamma}{\gamma - 1}\left[\left(\frac{p_2}{p_1}\right)^{(\gamma-1)/\gamma} - 1\right]$$

$$\text{where} \quad p_1 = p_w,\ p_2 = p_{ch} \text{ and } \quad \gamma = \frac{c_p}{c_v} = 1.4 \tag{2}$$

The speed range considered was 30 000 rpm to 50 000 rpm, which corresponded to a peripheral speed of 99 m s^{-1}–165 m s^{-1} and the air gap range was chosen to be between 0.6 mm to 1.5 mm. These ranges were considered to be representative of the values relevant to industry.

Each experiment was repeated three times in order to achieve a statistically representative result and the data presented here were the arithmetic mean of the repeated runs.

4. Results and discussion

4.1. Wheel speed vs pumping power

Fig. 5 shows the typical behaviour of the pumping power with wheel speed and air gap for the 4 × Ø4 mm wheel and the general trend observed is an increase of pumping power with wheel speed and air gap. This trend was also present in the data obtained for the other wheels considered. An unexpected trend is the localised minima at speeds of 30 000 rpm to 40 000 rpm which became less marked at larger air gaps. It is proposed that this was due to an observed physical closure of the wheel air gap occurring at these speeds. A degree of axial movement was present in the shaft assembly, estimated at 0.3 mm, which allowed the shaft to move vertically upwards within the housing thereby reducing the air gap which was set with the wheel stationary. This play was believed to be present in order to allow for thermal expansion when the atomiser is running for extended periods within a high temperature air stream.

The mechanism of gap closure was thought to be due to two contributory actions, namely an axial thrust generated by the pair of parallel helical spur gears and the axial force generated by the presence of a vacuum on the wheel top side and the positive chamber pressure on the wheel underside. The forces due to these actions were estimated at 0.4 N and

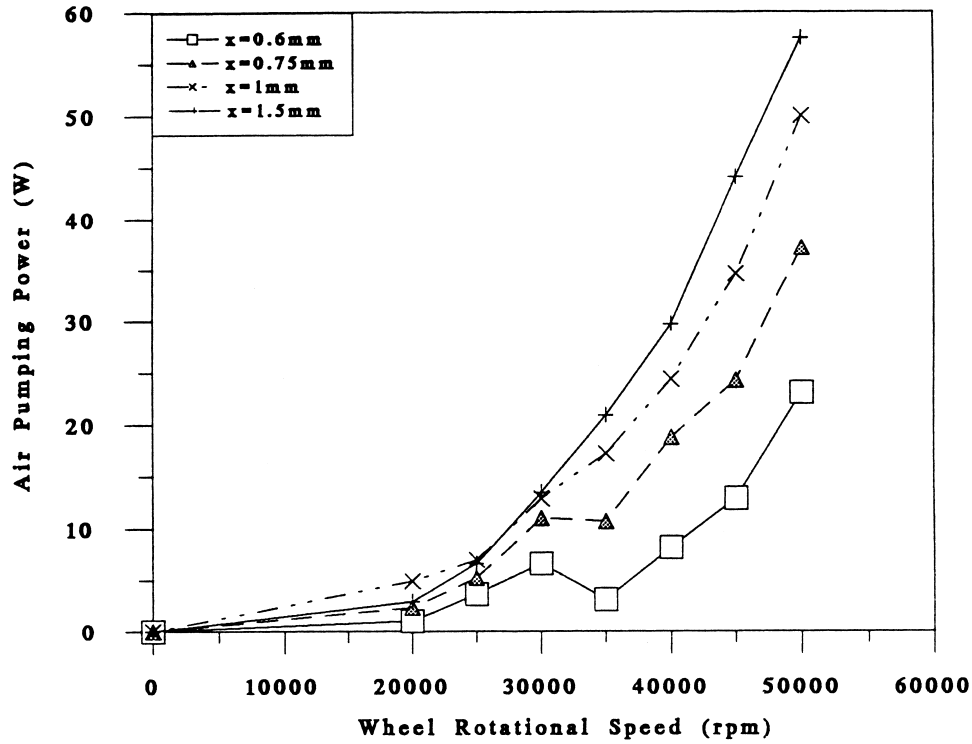

Fig. 5. Air pumping power variation with wheel speed and air gap for the atomiser wheel with 4 × Ø4 mm ports.

3 N, respectively, which would be sufficient to raise the shaft assembly which weighed ≈3 N.

An opportunity was taken to compare the measured shear power W_s with a theoretical model based on boundary layer theory. Appendix B details this model which took the form of a combination of expressions for power required to shear the fluid on the upper and lower surfaces of the wheel [7],

$$W_s = 0.073\rho\Omega^3 R^5 \left(\frac{\mu}{R^2\Omega\rho}\right)^{1/5} \quad (3a)$$

and the power required to shear the peripheral surface of the wheel,

$$W_s = 0.13\rho\Omega^3 R^4 b \left(\frac{\mu}{R^2\Omega\rho}\right)^{1/5} \quad (3b)$$

Fig. 6 shows the comparison of the measured shear power with this expression. It can be seen that the theoretical expression predicted ≈20% less power than was measured at 50 000 rpm. This could be accounted for by consideration of the complex convective flow cell within the wheel air gap departing from the basis of expressions 3a and 3b. Hence, it is reasonable to suggest that this form of modified model could be used to accurately predict the shear power for this and other wheel designs.

4.2. Wheel speed vs pressure difference

The typical behaviour of the wheel pressure differential with wheel speed and air gap is shown in Fig. 7 and the general trend observed is an increase of pressure difference (i.e., a decrease of pressure at the wheel centre) with wheel speed and a decrease with air gap. The latter effect is due to the increased resistance to flow through the air gap as the gap narrowed. Again, the influence of the closure of air gap can be seen as the data diverges at wheel speeds between 30 000 rpm and 35 000 rpm.

Interestingly, the pressure differential across the wheel within this speed range corresponds to ≈2 kPa. It is estimated that this pressure difference across the upper and lower surfaces of the wheel generates an upthrust of ≈3 N. This corresponds to the weight of the wheel and shaft assembly which reinforces the proposal made above, in which the governing mechanism in gap closure was the force generated by the pressure differential between the upper and lower surface of the wheel.

4.3. Wheel speed vs pumped flowrate

Figs. 8–10 illustrate the behaviour of the pumped flowrate with wheel speed and air gap for the 4 × Ø2 mm, 8 × Ø2 mm and 4 × Ø4 mm wheels and the general trend observed was an increase of flowrate with wheel speed and air gap. Again the influence of the gap closure can be seen as a reduction in the pumped air flowrate between the speed range from 30 000 rpm to 40 000 rpm. The effect of the gap closure becomes less marked at larger values of original gap size. This is due to the smaller percentage reduction in gap flow area as the prescribed gap size increases.

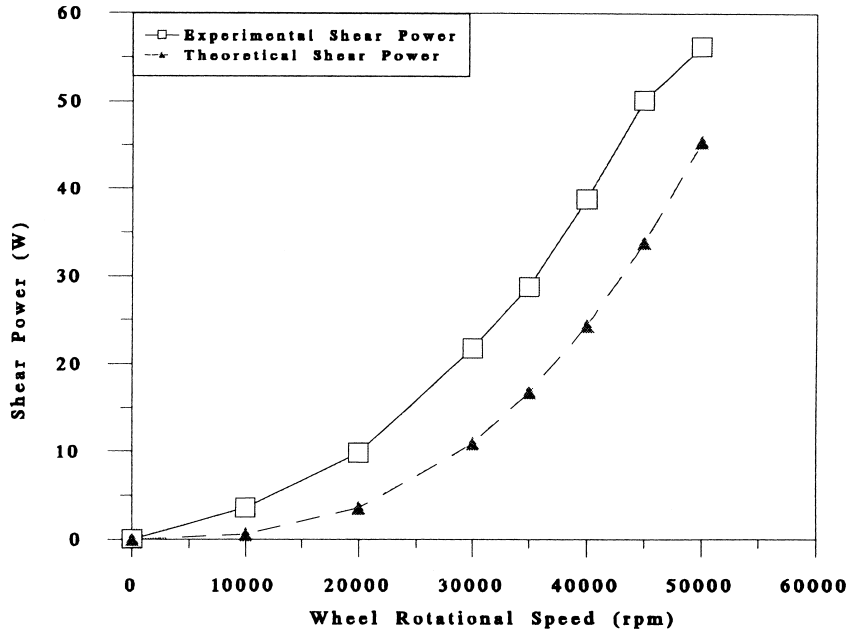

Fig. 6. Comparison of experimentally measured shear power and a theoretical expression derived from boundary layer considerations (expressions 3a and 3b).

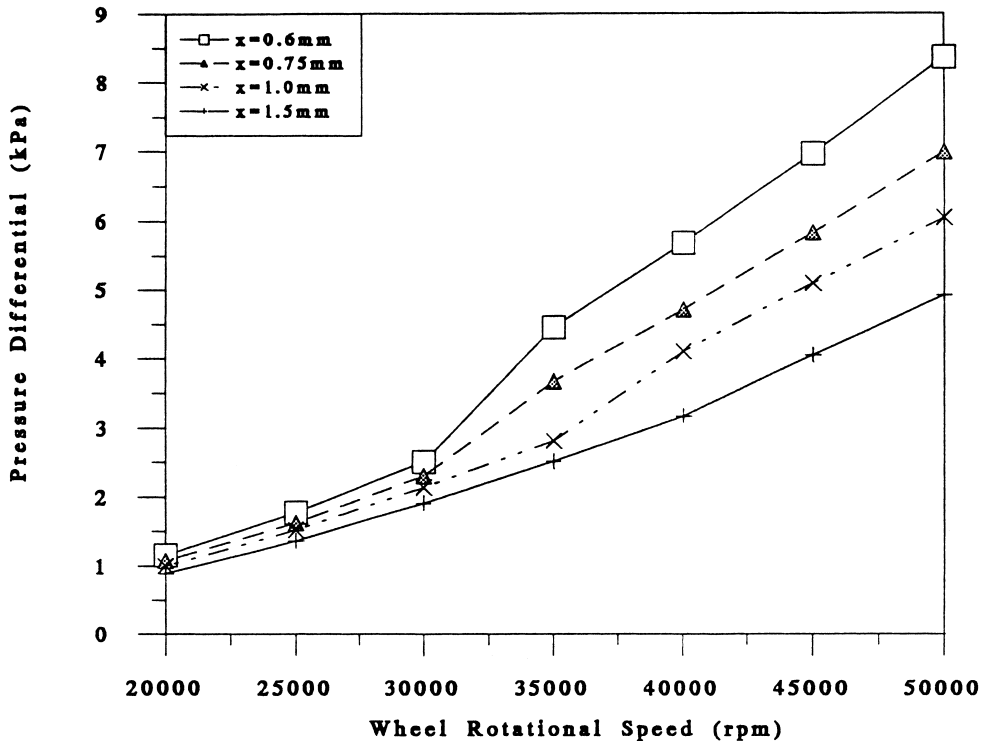

Fig. 7. Variation of wheel pressure differential with wheel speed and air gap for the atomiser wheel with 4 × Ø4 mm ports.

The maximum air velocities within the ports corresponding to these flowrates are shown in Table 1.

It can be seen that the Mach numbers are greater than 0.2 which reinforces the decision to consider the air-pumping process in a wheel of this size to be approximated by an adiabatic compression process.

As two flow paths were present i.e., the air gap path and the port path, it was decided to investigate which one, if any, controlled the flow process. In order to do this the sensitivity of the pumped airstream to increments in the air gap and the port flow area were considered. These are shown in Figs. 11 and 12, where it can be seen that the flow within the

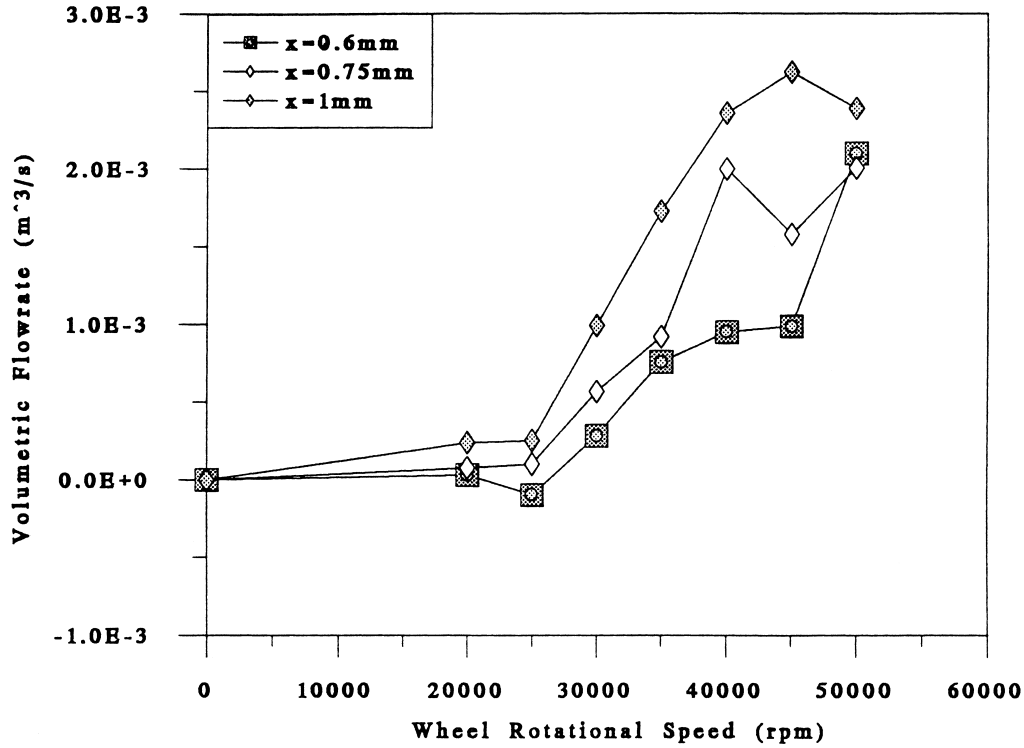

Fig. 8. Variation of pumped air flowrate with wheel speed and air gap for the atomiser wheel with 4 × Ø2 mm ports.

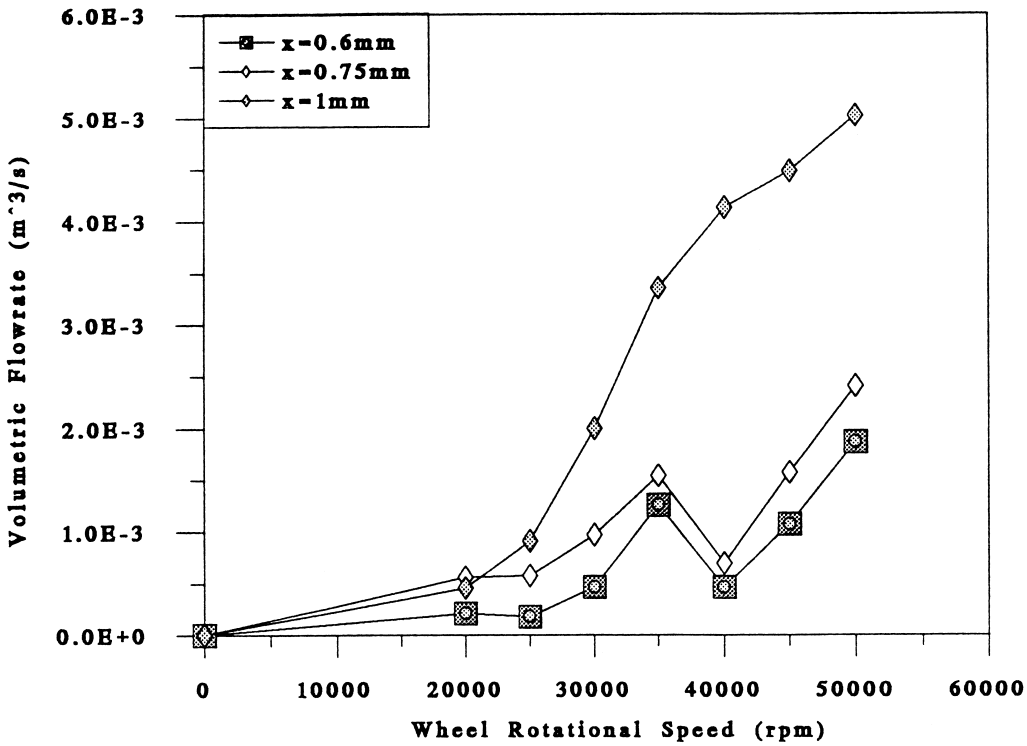

Fig. 9. Variation of pumped air flowrate with wheel speed and air gap for the atomiser wheel with 8 × Ø2 mm ports.

4 × Ø2 mm wheel appears to be relatively insensitive to changes in the air gap size which suggests that in this case the port circuit controls the flow. This is reinforced when the 8 × Ø2 mm wheel is used (100% increase in port circuit flow area) under the same conditions at which point the flowrate increases by 100%. Increments in air gap for this wheel produce a much greater increase in flowrate which suggests that the influence of the air gap path on the flow is

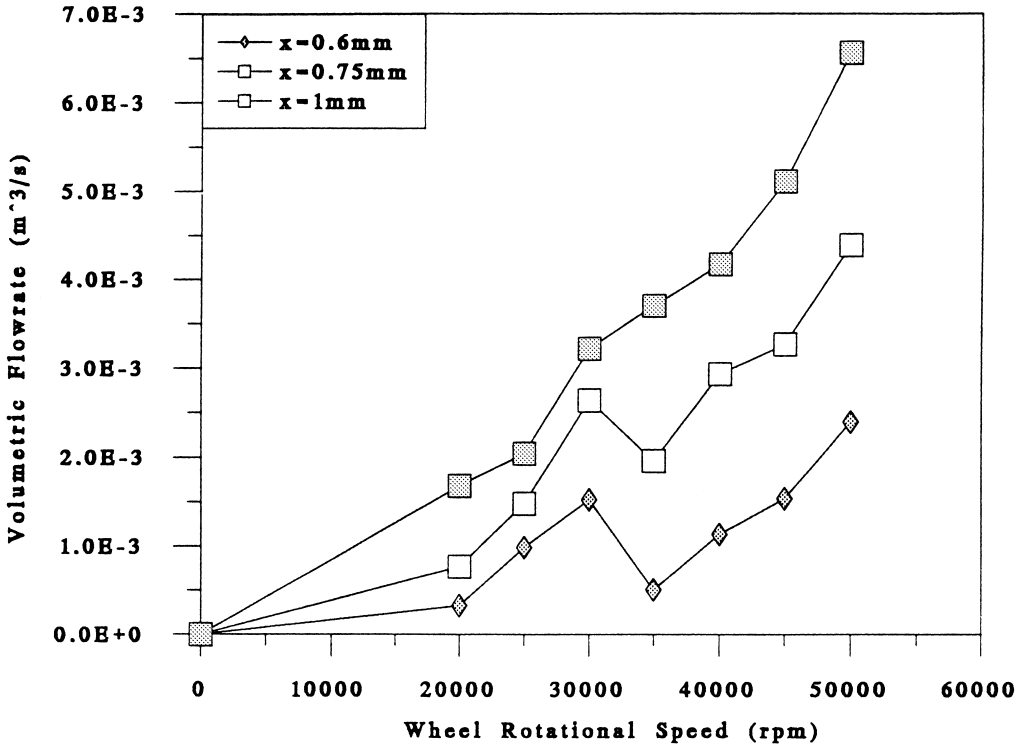

Fig. 10. Variation of pumped air flowrate with wheel speed and air gap for the atomiser wheel with 4 × Ø4 mm ports.

Table 1
Mean air velocities assuming plug flow within wheel ports corresponding to maximum pumped air flowrates

No. ports × port dia	Max. pumped flowrate l s^{-1}	Mean port air velocity m s^{-1}
4 × Ø2 mm	2.1	167 (Ma = 0.47)
8 × Ø2 mm	5.0	199 (Ma = 0.56)
4 × Ø4 mm	6.6	131 (Ma = 0.37)

on the increase. A further increment in port flow area with the 4 × Ø4 mm wheel (a 100% increase in flow area compared with the 8 × Ø2 mm wheel) resulted in only a 30% increase in flowrate, whereas increments in air gap continued to substantially influence the pumped flowrate. This suggests that both flow paths have similar dominant effects on the flow process.

4.4. Modelling the air gap flow path

In order to accurately model the air pumping phenomenon it would be necessary to take a combined account of the three-dimensional air flow within the wheel gap, the compressible nature of the flow within the wheel ports and the rotodynamic characteristics of the wheel. This topic is out of the domain of this paper, however, some of these topics have received attention elsewhere [5].

Fundamental to any combination of the approaches described above is a model of the flow circuit within the air gap. This is reinforced by the data shown in Figs. 11 and 12 where the gap flow path is seen to be a flow controlling path. A simplistic analytical model of the flow path was developed which considered the flow within the gap to be purely two-dimensional and incompressible. This last assumption is a reasonable one to make as the Mach number within the gap ranges was found to vary between 0.08 to 0.22.

The flow model consisted of the application of Bernoulli's equation along the air gap flow path. An account was taken of the pressure losses due to friction and 'fitting' losses through the use of standard empirical correlations for friction factors and loss coefficients, as well as pressure and velocity changes due to cross-sectional changes. More details of this model can be found in Appendix A.

The model was used to determine the pressure difference-flowrate relationship for the flow path within the air gap. The experimental values of flowrate were used within the model to yield a comparable wheel pressure difference and hence wheel centre pressure value. Fig. 13 shows a comparison of the measured and derived air pressures at the wheel centre and it can be seen that the dynamic closure of the wheel gap, which is not taken account of within the model, significantly affects its performance. Prior to the gap closure the model underpredicts the vacuum pressure at the wheel centre by an offset of ≈1000 Pa. Once closure occurs this under-prediction increases to ≈4000 Pa. It is likely that if the actual gap size that the rotating wheel possessed was used instead of the initially set value then the disparity with the measured value could be reduced to the typical levels before gap

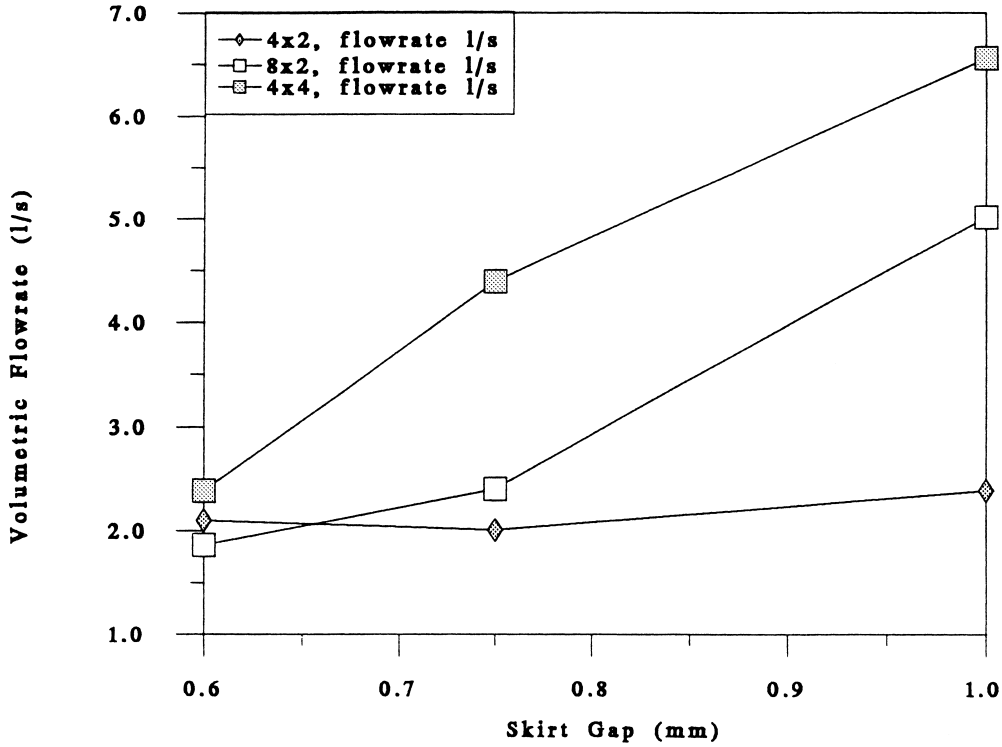

Fig. 11. Volumetric flowrate as a function of skirt gap.

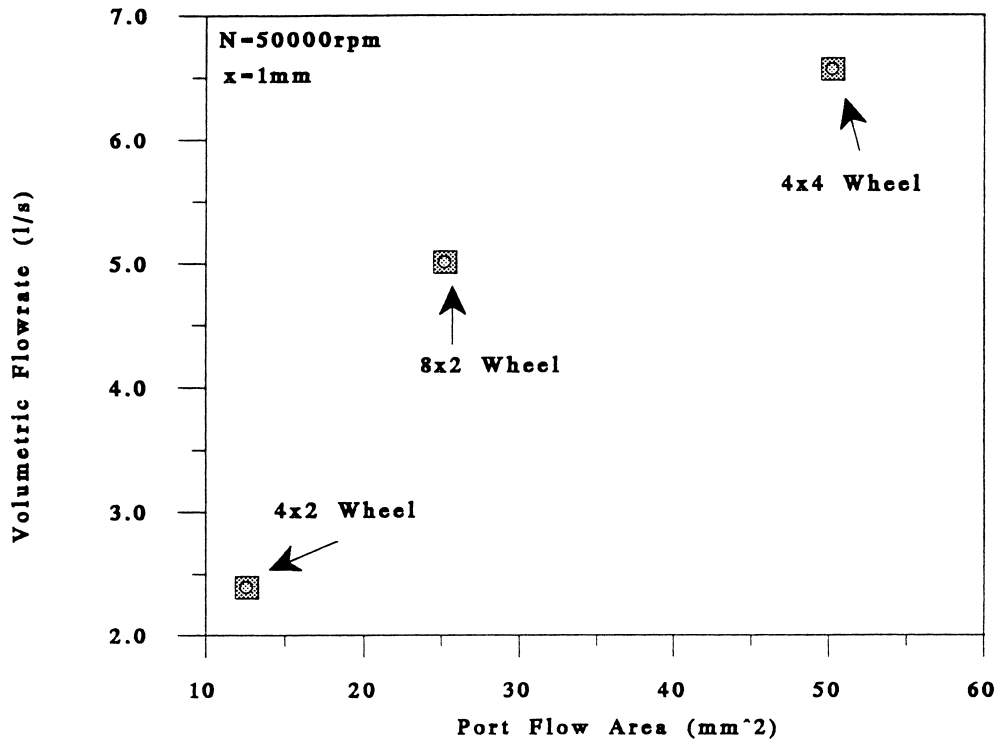

Fig. 12. Pumped air flowrate for the 4 × Ø2 mm, 8 × Ø2 mm and 4 × Ø4 mm wheels showing the influence of port flow area.

closure. It is considered that the assumption of pure radial flow within the air gap, as well as the measuring point for the central wheel pressure not being at the same spatial location as the perceived section used in the model, were the reasons behind the disparity between the measured and calculated data.

Significant improvements within this model would have to be made before it could be integrated with a system of

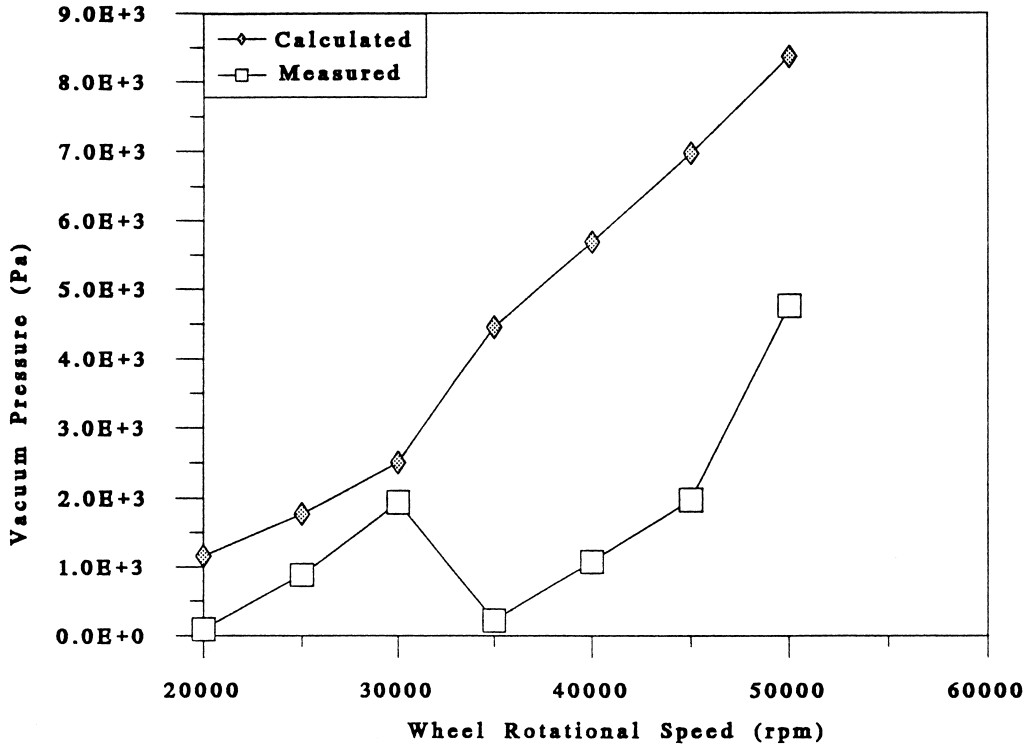

Fig. 13. A comparison of the measured and calculated vacuum pressure at the wheel centre showing the predictive model's inability to account for the dynamic gap closure (4 × Ø4 mm wheel, air gap $x = 0.6$ mm).

equations which would take account of the centrifugal pumping effect, most likely represented by a derivative of Euler's equation for hydrodynamic machinery in order to explicitly predict the pumped flowrate within such an atomiser wheel.

5. Conclusions

The experimentally derived values of pumped air flowrate were found to be between 5% and 16% of the primary air flowrate through the dryer. These values were lower than those found by Keey et al. [5] who considered a wheel of larger diam (120 mm). These authors did not take account of an additional source of power loss which would not contribute to air pumping, which would be liable to significantly reduce the amount of air pumped. This trend of reduced relative amounts of air pumping with increasing wheel size is consistent with Masters [1] who suggests that the magnitude of air pumping diminishes with wheel size and the corresponding influence of the pumped air stream on the dryer flow diminishes with increasing dryer size.

Although the flow of air through the wheel was a function of wheel speed, the flow process was strongly influenced by the size of both the port and gap flow paths. Readings of air flowrate with an atomising liquid present were not possible, however this result reinforces the standard operating practice of running such an atomiser with the minimum practicable gap in order to reduce air pumping, whatever the wheel speed.

The relative magnitudes of the pumped air stream flowrate and momentum, which are of the same order as those possessed by the primary air stream within the dryer, suggest that their influence on the dryer flow patterns would indeed be substantial and that it would be prudent to account accurately for their presence when simulating such flows, using for example CFD codes.

The issue of the amount of air pumped when such a wheel is running with a liquid present still requires substantial investigation, however if similar quantities of air are pumped under conditions of liquid loading then the momentum of the emerging spray/pumped-air stream would be substantially more (perhaps 2–3 times) than that possessed by the spray alone, which again would have a substantial effect on the dryer flow field. It is likely that the presence of a liquid within the wheel would have the effect of reducing the port flow area available for pumped air flow and consequently reducing the amounts of pumped air present. Combining the reduction of the relative rates of air pumping as wheel and dryer scale increase together with the reduction in pumped air flowrates due to liquid loading, it is likely that air pumping has a less substantial effect on dryer flow fields in large industrial scale dryers. However in situations where small scale dryers are the industrial norm, i.e., in the drying of high value added pharmaceuticals and catalyst, then the impact of air pumping may still be substantial.

6. Nomenclature

A	cross-sectional flow area (m^2)
b	wheel axial thickness (m)
c_p	specific heat capacity at constant pressure (J/kgK)
c_v	specific heat capacity at constant volume (J/kgK)
d_e	equivalent hydraulic diameter (m)
f	friction Factor (–)
g	acceleration due to gravity (m/s^2)
h	gravimetric head (m)
h_l	head loss due to friction losses in flow path of length l (m)
k	loss coefficient (–)
l	length of flow path (m)
Ma	mach number (–)
n	index of position within wheel air gap (–)
N	wheel rotational speed (rpm)
p	pressure (Pa)
p_{ch}	chamber air pressure (Pa)
p_w	air pressure at wheel centre (Pa)
Δp_1	pressure difference between the wheel centre and the chamber bulk (Pa)
Q	volumetric flowrate ($m^3\ s^{-1}$)
r	radius (m)
R	wheel radius (m)
Re	Reynolds number (–)
u	fluid velocity (m s)
$\bar{u}$	mean fluid velocity (m s)
W_f	power consumed due to fluid friction (W)
W_p	power consumed due to air pumping (W)
W_s	power consumed due to shear flow (W)
x	wheel air gap (m)

Greek letters

γ	Ratio of specific heat capacities, c_p/c_v (–)
μ	Fluid dynamic viscosity ($kg\ ms^{-1}$)
ν	Fluid kinematic viscosity ($m^2\ s^{-1}$)
ρ	Fluid density (kg/m^3)
Ω	Wheel rotational velocity (rad/s)

Acknowledgements

The Engineering and Physical Science Research Council are gratefully thanked for funding this work under Grant No: GRJ 76682. The authors would like to acknowledge the support of APV Anhydro A/S, Copenhagen, Denmark, who provided the spray dryer and atomisation equipment for use in this study and Dr. Norman Macleod, University Fellow, The University Of Edinburgh for discussions relating to this work. Finally, the publication referees are thanked for their very helpful comments which improved the work reported herein.

Appendix A

A flowrate-pressure difference model for the air flow path

If we make the assumption that the air is drawn into the gap with a radial velocity component only, then we can define the pressure variations at various points within the gap by applying Bernoulli's equation accounting for pressure losses due to friction and fitting losses. The general form of this equation applied between positions n and $n+1$ is as follows,

$$p_n + 0.5\rho u_n^2 + \rho g h_n = p_{n+1} + 0.5\rho u_{n+1}^2 + \rho g h_{n+1} + \Delta p_{(n+1)-n} \quad (A.1)$$

where the pressure loss $\Delta p_{(n+1)-n}$ is estimated either by an appropriate loss coefficient k or in the case of a frictional loss, by Darcy's equation. Values of k and friction factor were taken from the literature [8].

Referring to Fig. 14, we can estimate $\Delta p_{(n+1)-n}$ between positions within the air gap as follows.

1-2

We define P_1 as the chamber pressure P_{ch}. The pressure drop from 1–2 can be considered to be that of an entry loss from an infinite reservoir to a finite channel, defined by,

$$\Delta p_{1-2} = 0.5k\rho u_2^2 \quad (A.2)$$

where $k = 0.5$.

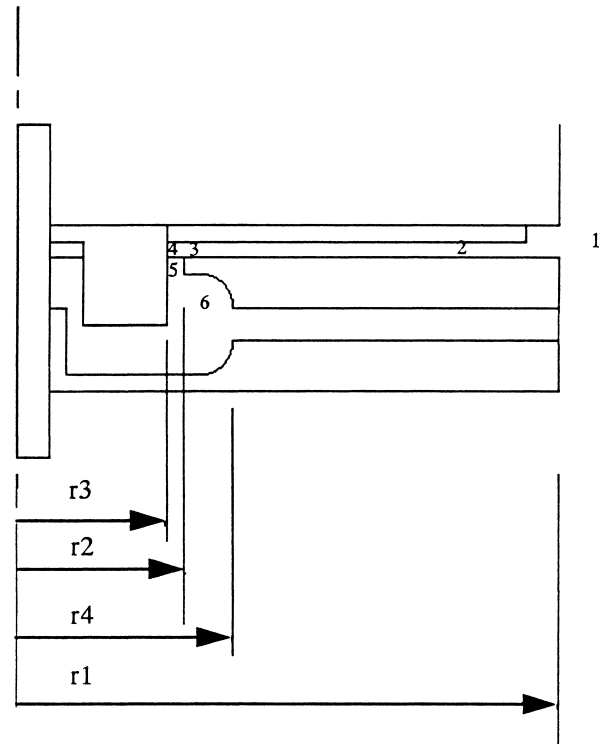

Fig. 14. Schematic of atomiser wheel showing radial positions used in the predictive model.

The entry is considered to be directly into the gap i.e., the constriction of the shoulder of the gap is ignored.

2-3

This is considered to be a narrow channel with pressure drop due to an associated friction factor calculated by Darcy's equation, thus,

$$h_l = \frac{4fl\bar{u}^2}{2d_e g} \tag{A.3}$$

where the friction factor f is defined by Blasius' equation,

$$f = 0.079\,\mathrm{Re}^{-0.25} \tag{A.4}$$

The Reynolds number Re is defined by

$$\mathrm{Re} = \frac{\rho\bar{u}d_e}{\mu} \tag{A.5}$$

and,

$$d_e = 2x \tag{A.6}$$

where x is the set air gap thickness.

The flow path length l was defined as,

$$l = r_1 - r_2 \tag{A.7}$$

The mean flow velocity was defined as the arithmetic mean of the gap inlet and outlet velocities, thus,

$$\bar{u} = \frac{u_2 + u_3}{2} = \frac{Q/2\pi r_1 x + Q/2\pi r_2 x}{2} = \frac{Q(r_1 + r_2)}{4\pi r_2 r_1 x} \tag{A.8}$$

3-4

This was approximated by a constant cross-section 90° bend with a loss coefficient of 1.2.

4-5

Approximated to a flow constriction into the throat of the annular constriction with a loss coefficient of 0.5.

$$\Delta p_{4-5} = 0.5\frac{u_5^2\rho}{2} \quad \text{where} \quad u_5 = \frac{Q}{\pi(r_2^2 - r_3^2)} \tag{A.9}$$

5-6

The flow expansion on outlet of the annular constriction was approximated by a rapid expansion with the following expression.

$$\Delta p_{5-6} = \frac{Q^2\rho}{2A_5^2}\left[\frac{A_5^2}{A_6^2} - 1\right]^2 \tag{A.10}$$

$$\text{where} \quad A_5 = \pi(r_4^2 - r_3^2) \tag{A.11}$$

$$\text{and} \quad A_6 = \pi(r_2^2 - r_3^2) \tag{A.12}$$

Position 6 was considered to be closest to the central region of the wheel where the measured pressure p_w was taken. Expression (4) was applied between positions 1–6 taking account of changes in fluid velocity due to cross-sectional variations thereby creating a means of predicting p_6 as a function of pumped air flowrate.

Appendix B

Derivation of power required to shear flow at the wheel surfaces (Eqs. (3a) and (3b)).

Consider the external surface of a solid cylinder of radius R and thickness b. If we define v as the velocity relative to an observer who is stationary on the surface of the rotating cylinder, then the skin friction force D, on the external surface due to the shear stress τ is,

$$D = b\tau 2\pi R \tag{B.1}$$

A momentum balance through the boundary layer of height δ above the cylinder surface yields,

$$D = b\rho\int_0^\delta v(v_\infty - v)\,\mathrm{d}y \tag{B.2}$$

where y is the distance in the radial direction from the wheel surface and v_∞ is the fluid velocity in the bulk fluid relative to the wheel surface, defined as,

$$v_\infty = R\Omega \tag{B.3}$$

If we assume a 1/7th power law for the velocity profile within the boundary layer, where the relative fluid velocity, v at a height y is given by,

$$v = v_\infty\left(\frac{y}{\delta}\right)^{1/7} \tag{B.4}$$

then substitution into the expression within the integral sign in Eq. (B.2) yields,

$$\int_0^\delta v(v_\infty - v)\,\mathrm{d}y = 0.0972\delta v_\infty^2 \tag{B.5}$$

Equating Eqs. (B.1) and (B.2) and substituting with Eq. (B.5), gives

$$\delta = 1.364R\left(\frac{\nu}{Rv_\infty}\right)^{1/5} \tag{B.6}$$

Schlichting [7] gives an expression for the shear stress within a boundary layer for a flat plate, which is a good approximation to the peripheral surface of the wheel, thus

$$\tau = 0.0228\rho v_\infty^2\left(\frac{\nu}{v_\infty\delta}\right)^{1/4} \tag{B.7}$$

Substituting Eqs. (B.6) and (B.7) into (Eq. (B.1)) gives,

$$D = 0.13Rb\rho v_\infty^2\left(\frac{\nu}{Rv_\infty}\right)^{1/5} \tag{B.8}$$

The associated power required to rotate the wheel at Ω rad/s due to skin friction at the periphery only is

$$W_1 = DR\Omega = 0.13\rho\Omega^3 R^4 b\left(\frac{\nu}{R^2\Omega}\right)^{1/5} \quad \text{(B.9)}$$

Furthermore an account of the additional power consumed due to skin friction along the upper and lower surfaces of the wheel can be made by consideration of the wheel as a thin circular disc immersed in a large body of fluid again assuming a 1/7th power velocity distribution within the turbulent boundary layer [7],

$$W_2 = 0.073\rho\Omega^3 R^5\left(\frac{\nu}{R^2\Omega}\right)^{1/5} \quad \text{(B.10)}$$

Therefore the total power consumed in rotating a wheel of radius R, thickness b at Ω rad/s is,

$$W_s = W_1 + W_2 \quad \text{(B.11)}$$

References

[1] K. Masters, Spray Drying Handbook, Longman Scientific and Technical, UK, 5th ed., 1991.

[2] D. Reay, et al., User Guide to fire and explosion hazards in the drying of particulate materials, Institution Of Chemical Engineers, 1977.

[3] R.A. Stafford, The measurement and utilisation of spray dryer residence time distribution, Ph.D. Thesis, Napier University, Edinburgh, Scotland, 1994.

[4] T.A.G. Langrish, R.B. Keey, C.A. Hutchinson, Flow visualisation in a spray dryer fitted with a vaned-wheel atomiser: photography and prediction. Trans. I. Chem. E, vol. 70 part A, pp. 385–394, July 1992.

[5] R.B. Keey, S.S. Enevoldsen, C. Werner, The air-pumping behaviour of rotary atomizers, in: A.S. Mujumdar, I. Filkova (Eds.). Drying 91, Elsevier, Amsterdam, pp. 314–323, 1991.

[6] K.E. Bett, J.S. Rowlinson, G. Saville, 1975. Thermodynamics for Chemical Engineers, The Athlone Press, London.

[7] H. Schlichting, Boundary Layer Theory, McGraw-Hill, New York, 1979.

[8] B.S. Massey, Mechanics of fluids, Van Nostrand Reinhold, UK, 1983.